Optica Applicata, Vol. LV, No. 3, 2025
DOI: 10.37190/oa/203360

Enhanced refractive index sensor based on annular porous silicon 1D photonic crystal for pathogen bacteria detection

Ayman A. Ameen[1], Amrindra Pal[2], Ahmed M. El-Sherbeeny[3], Arun Uniyal[4], Mostafa R. Abukhadra[5], Jacob Wekalao[6], Wail Al Zoubi[7], Ahmed Mehaney[8], Hussein A. Elsayed[8,*]

[1] Physics Department, Faculty of Science, Sohag University, Sohag, 82524, Egypt

[2] University Centre for Research and Development, Chandigarh University, Gharuan, Mohali 140413, India

[3] Industrial Engineering Department, College of Engineering, King Saud University, P.O. Box 800, 11421, Riyadh, Saudi Arabia

[4] Department of Electronics and Communication Engineering, Institute of Technology Gopeshwar, Chamoli, Uttrakhand-246424, India

[5] Materials Technologies and their applications Lab, Faculty of Science, Beni-Suef University, Beni Suef city, Egypt

[6] Department of Optics and Optical Engineering, University of Science and Technology of China, Hefei 230026, China

[7] Materials Electrochemistry Laboratory, School of Materials Science and Engineering, Yeungnam University, Gyeongsan, 38541, Republic of Korea

[8] Physics Department, Faculty of Science, Beni-Suef University, Beni-Suef 62512, Egypt

[*] Corresponding author: drhussien85sc@gmail.com

This work presents a novel approach for pathogen identification using a one-dimensional annular photonic crystal (APC). The APC structure consists of alternating silicon layers with varying porosities arranged in a periodic pattern. A defect layer has been incorporated for the detection and monitoring of *E. Coli* bacteria. The optical characteristics of the APC are analyzed by solving Maxwell's equations and employing the modified transfer matrix method in Cartesian coordinates. The proposed APC design, which features a configuration of (layer a/layer b)^N/defect layer/(layer a/layer b)^N, demonstrates promising potential for pathogen detection when using water and *E. Coli* samples in the defect layer alongside porous silicon in a multilayer stack. All design parameters are meticulously optimized to achieve peak sensor performance. Various performance metrics, including resonant peak position, quality factor, figure of merit, and sensitivity, are calculated. Numerical simulations and theoretical analyses provide insight into the interaction between pathogenic microorganisms and the APC. This research contributes to the development of sensitive and effective optical sensing technologies for pathogen detection across various applications. Our design achieves a sensitivity of 231.4 nm/RIU and a quality factor of 667.5.

Keywords: photonic crystals, annular photonic crystal, sensor, sensitivity, reflectance, photonic band gap, figure of merit, quality factor.

1. Introduction

Photonic crystals (PCs) have played a crucial role in the design and development of various physical, optical, and technological applications over the past thirty years. In these applications, the primary function of PCs is related to the attenuation or trapping of electromagnetic radiation. The reduction of incident light within a specific frequency range is mainly attributed to the formation of certain frequency bands known as photonic band gaps (PBGs) [1-4]. These PBGs are created by the heterostructure of PCs, which can be constructed from two or more materials with different optical properties [5-7].

Additionally, modifying the periodicity of PCs may result in the light trapping of the incident radiation [8-10]. Dielectrics, semiconductors, metals, superconductors, graphene, and nanocomposites are among the materials that are frequently taken into account when determining the tunability of PBGs and light trapping [11-13]. The emergence of resonant defect modes has drawn a lot of interest recently in the fields of PCs, optical, and biosensing because of their significant impact on these sensors' performance and experimental findings. According to reports, these occurrences may also greatly improve the sensors' sensitivity and quality factor [14-18]. Thus, numerous applications, including gas sensing [18], biological sensing [19], optical filters [20], light -emitting devices [21], solar cells [22], and optical switches [23] have been introduced based on the emergence of these resonant modes.

On the other hand, a new geometry that offers greater comfort and simplicity is required for the fabrication process. 1D annular PCs (1D APCs) solve fabrication issues that may arise with 1D planar PCs [17,18]. In addition to having accurate measuring capabilities, such structures could be made more realistic during fabrication, particularly for certain chemical and biological applications. The 1D multilayer structures with a cylindrical shape could be used to construct circular PCs. Furthermore, as shown by KLIMOV *et al*., the well-known transfer matrix method (TMM) might be modified to provide a theoretical analysis of the interaction of electromagnetic waves with these structures [23]. In this context, the inclusion of annular geometry received a significant contribution in the design of different physical and biomedical and chemical applications [24-27]. ABADLA *et al*., demonstrated the thermal properties of the 1D APCs based on some materials that their optical properties can be effectively tuned due to the temperature variations [25,26]. Accordingly, the designed structure can be introduced as a temperature sensor of sensitivity = 0.224 nm/°C [25]. In contrast, SAYED *et al*., have introduced the 1D APCs to act as a salinity sensor providing a sensitivity of 782 nm/RIU [24]. In addition, GANDHI *et al*., have demonstrated a multilayers design of annular geometry based on SiO_2 and TiO_2 materials as a biosensor to detect the bacteria cells and spore present in water sample [27]. Based on these significant contributions, we believe that the dependence on the annular geometry in the sensing and monitoring applications could be of a promising interest. Notably, this geometry may represent the key link between the 1D PC designs and PC fibers. Thus, we have intro-

duced in the present communication a simple 1D APC structure as a biosensor to detect the different concentrations of *Escherichia Coli* (*E. Coli*) bacteria in pure water.

In particular, the developing of photonic optical sensors to detect pollution is extremely desirable. It has been suggested that photonic sensing technology can be used to identify pollutants or harmful germs in food and water [1,27]. The public health of the world is seriously threatened by the quick evolution of bacteria resistant to antibiotics. For efficient disease treatment and prevention, these infections must be detected accurately and promptly. Conventional diagnostic techniques, like biochemical testing and culturing, are frequently labor-intensive and time-consuming. As a result, creative and effective methods for pathogen identification are desperately needed. There is a dangerous type of bacteria, which is named as *E. Coli*, is one of these types of bacteria that must be detected through the outgoing designs of PCs. Most *E. Coli* germs are mainly found in animal and human intestines [28,29]. Water sources, such as wells tainted with animal or human excrement, may harbour *E. Coli* O157:H7 [30]. Enzyme-producing bacteria *E. Coli* are classified as the most pathogenic organisms in the *Enterobacteriaceae* family of gram-negative bacteria [31]. *E. Coli* in water is a sign of animal and human faces pollution. Consequently, it is imperative to identify *E. Coli* bacteria to preserve public health and water quality. Xin *et al*. introduced research for monitoring of bacteria using electro-photonic traps [32]. They predicted a variation in measurable electrical current of up to 40% between dead and live bacteria. Also, Lin *et al*. presented a review study with nanomaterials-based optical biosensors for the detection and discrimination of pathogenic bacteria [33]. Although these valuable studies rely on optical designs to detect bacteria, many of them suffer from high costs, low sensitivity, and a lack of performance calculations. Therefore, it is essential to develop highly sensitive sensors based on PCs, specifically active PCs, for the detection of *E. Coli* due to their superior sensitivity and selectivity [24-26].

Meanwhile, we have introduced in this research paper a novel approach for pathogen identification using a 1D APC. The designed APC structure consists of alternating porous silicon layers with varying porosities arranged in a periodic pattern. A defect layer has been incorporated for the detection and monitoring of *E. Coli* bacteria. Therefore, the proposed APC design, could be introduced as, (layer a/layer b)^N/defect layer/(layer a/layer b)^N. To optimize the proposed sensor regarding the best performance of the designed sensor, we conduct numerous optimization steps focusing on various geometric parameters. The organization of this research is as follows. Section 2 discusses the theoretical framework and fundamental equations of the transfer matrix method (TMM) in cylindrical coordinates. Additionally, the equations relating the optical properties (refractive index *versus E. Coli* concentration) are presented in this section. In Section 3, we analyze the results by plotting the reflection spectra against the operating wavelength for each geometric parameter. We also examine factors influencing the sensor's performance, including detection limits, signal-to-noise ratios, quality factors, sensitivity, and figures of merit for different levels of porosity and defect layer thicknesses. Finally, the Conclusion section summarizes the key findings from the results.

2. Proposed design with mathematical analysis

Figure 1 displays the schematic diagram of 1D APCs. The design consists of a starting section, or innermost circular portion, with a radius of γ_0 and a refractive index (RI) of n_0. Notably, the circular area of a radius γ_0 represents the area at which the source of the incident electromagnetic waves can be placed to interact with the designed structure. Meanwhile, this circular area represents the starting medium of the incident electromagnetic waves and was expressed as air of a refractive index $n_0 = 1$. Then, layer 'a' is designed from porous silicon of porosity of 0.7 and layer 'b' is designed from porous silicon of porosity of 0.5 are deposited in alternating layers with RIs of n_1 and n_2, and optimum values of their thicknesses as $d_1 = 70$ nm and $d_2 = 75$ nm, respectively. To realise a defect peak in the reflectance spectrum, a defect layer with RI of n_d and thickness 48 nm is introduced into the suggested APC. The APC period preceding and succeeding the defect layer is N, where N is the structure's periodicity, here defined as 10.

Then, the modified TMM represents the mainstay of our theoretical formalism besides the optical properties of the constituent materials. The TMM involves representing each layer of the PC structure by a 2×2 matrix that relates the electric and magnetic

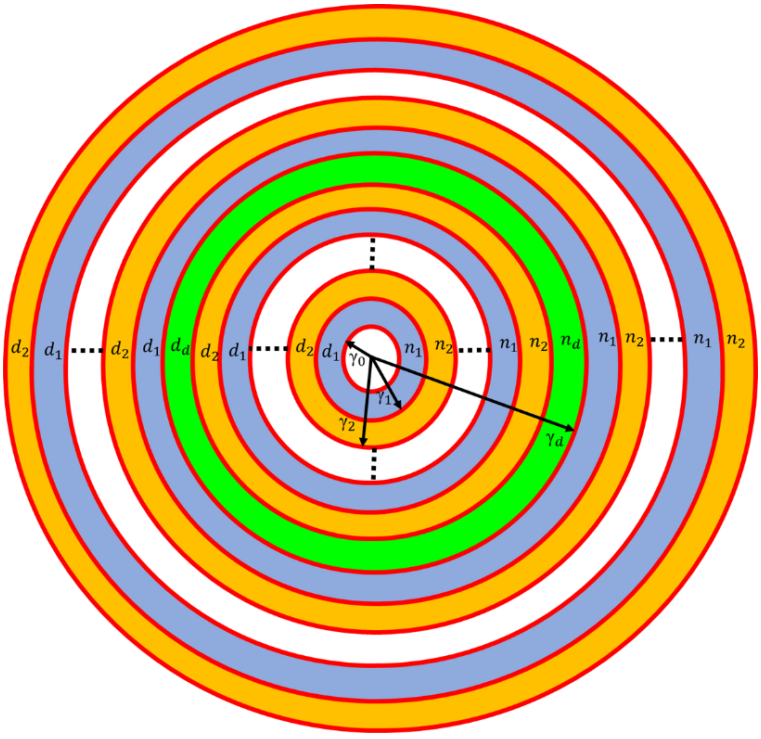

Fig. 1. Sensor schematic diagram of the 1D APCs in which two different materials of refraction indices (n_1 and n_2) and thicknesses (d_1 and d_2) are repeated for N periods before and after the defect layer. Here, γ_0 represents the radius of the inner core.

fields at the input and output interfaces of the layer [17,23-26]. The overall transfer matrix of the entire structure is obtained by multiplying the individual transfer matrices of each layer [23-26]. For a cylindrical geometry, the TMM can be formulated in terms of Bessel functions to account for the radial dependence of the electromagnetic fields. For this purpose, it is assumed that the cylindrical wave is incident normally on the initial contact at $\gamma = \gamma_0$ after diverging from the axis of symmetry at $\gamma = 0$. In the cylindrical Bragg wave, the reflectance at the initial circular boundary, $\gamma = \gamma_0 = 500$ nm, is calculated by using the TMM [17,23-26]. The TMM is used to look at how cylindrical electromagnetic waves propagate via each cylindrical interface for various azimuthal modes and polarisations. The proposed structure of the APC is then with the configuration (layer a/layer b)^N/defect layer/(layer a/layer b)^N. Where, the defect layer consists of water in addition to *E. Coli* samples with different volume fractions. The substrate layer is the outer area, or final medium, which has the RI of n_s. Here, the substrate material is considered as glass of refractive index, $n_s = 1.52$.

Given the assumption that each electromagnetic field's temporal component is $\exp(j\omega t)$, the source-free two curl Maxwell's equations are as follows:

$$\nabla \times \mathbf{E} = -j\omega\mu\mathbf{H} \tag{1}$$

$$\nabla \times \mathbf{H} = j\omega\varepsilon\mathbf{E} \tag{2}$$

where ω is the angular frequency. There are two feasible modes (or polarisations) for the cylindrical Bragg wave: the TE and TM modes. The non-zero fields for the TE wave are E_z, H_φ, and H_ρ, which fulfil the following equations in each monolayer:

$$\frac{1}{\rho}\frac{\partial E_z}{\partial \varphi} = -j\omega\mu H_\rho \tag{3a}$$

$$\frac{\partial E_z}{\partial \rho} = j\omega\mu H_\varphi \tag{3b}$$

$$\frac{\partial(\rho H_\varphi)}{\partial \rho} - \frac{\partial H_\rho}{\partial \varphi} = j\omega\varepsilon\rho E_z \tag{3c}$$

With the help of (3), the formula that governs for E_z can be found and is expressed by:

$$\rho\frac{\partial}{\partial\rho}\left(\rho\frac{\partial E_z}{\partial\rho}\right) - \rho^2\frac{1}{\mu}\frac{\partial\mu}{\partial\rho}\frac{\partial E_z}{\partial\rho} + \frac{\partial}{\partial\varphi}\left(\frac{\partial E_z}{\partial\varphi}\right) + \omega^2\mu\varepsilon\rho^2 E_z = 0 \tag{4}$$

Using the approach of separation of variables, the solution for E_z may be determined and is represented as:

$$E_z(\rho, \varphi) = V(\rho)\Phi(\varphi) = \left[AJ_m(k\rho) + BY_m(k\rho)\right]\exp(im\varphi) \tag{5}$$

where, m is the azimuthal number, $k = \omega\sqrt{\mu\varepsilon}$ is the medium's wave number, J_m is a Bessel function, Y_m is a Neumann function, and A and B are constants. Then, the azimuthal component of the magnetic field H_φ is obtained from (3b) as follows:

$$H_\varphi(\rho, \varphi) = U(\rho)\Phi(\varphi) = -\sqrt{\frac{\varepsilon}{\mu}}\left[AJ'_m(k\rho) + BY'_m(k\rho)\right]\exp(im\varphi) \tag{6}$$

Here, $k\rho$ indicates medium's intrinsic admittance. We can determine the single-layer matrix relationship between the electric and magnetic fields at its two interfaces with the use of Eqs. (5) and (6). With refractive index n_1 and interfaces at $\gamma = \gamma_0$ and γ_1, the matrix for the first layer T_1 may be expressed as:

$$\begin{bmatrix} X_{\gamma_1} \\ Y_{\gamma_1} \end{bmatrix} = T_1 \begin{bmatrix} X_{\gamma_0} \\ Y_{\gamma_0} \end{bmatrix} \tag{7}$$

$$T_1 = \begin{bmatrix} t_{11} & t_{12} \\ t_{21} & t_{22} \end{bmatrix} \tag{8}$$

The values of t_{11}, t_{12}, t_{13} and t_{14} can be obtained from [17,23-26]. The following expression can be used to determine the transmittance T and reflectance R of the APC:

$$R = \left|r_{\mathrm{d}}\right|^2 \tag{9}$$

$$T = \frac{n_f}{n_0}\left|t_{\mathrm{d}}\right|^2 \tag{10}$$

Just swapping out $\varepsilon \leftarrow \mu$ and $j \leftarrow -j$ in the TE wave calculation yields the reflectance and transmittance expression for the TM wave.

The matrix equation for the overall system matrix T is given by:

$$\begin{bmatrix} X_{\gamma_f} \\ Y_{\gamma_f} \end{bmatrix} = T_N \ldots T_3\, T_2\, T_1 \begin{bmatrix} X_{\gamma_0} \\ Y_{\gamma_0} \end{bmatrix} \tag{11}$$

$$\begin{bmatrix} X_{\gamma_f} \\ Y_{\gamma_f} \end{bmatrix} = M \begin{bmatrix} X_{\gamma_0} \\ Y_{\gamma_0} \end{bmatrix} \tag{12}$$

Meanwhile, Eqs. (9)–(12) represent the mainstay towards introducing both transmittance and reflectance of the considered 1D APC structure based on the optical properties of the constituent materials and their thicknesses as well besides the wavelengths of the incident electromagnetic radiation. Meanwhile, the indices of refraction for layers a and b can be expressed in terms of their porosities [34]. In this regard,

Bruggeman's effective medium approximation can be utilized to describe the effective refractive index of porous Si based on the porosity level such as [34]:

$$n_{\mathrm{pSi}} = 0.5\sqrt{\sigma + \sqrt{\sigma^2 + 8\, n_{\mathrm{Si}}^2\, n_{\mathrm{analyte}}^2}} \tag{13a}$$

$$\sigma = 3P\left(n_{\mathrm{analyte}}^2 - n_{\mathrm{Si}}^2\right) + \left(2n_{\mathrm{Si}}^2 - n_{\mathrm{analyte}}^2\right) \tag{13b}$$

where P, n_{Si} and n_{analyte} describe the porosity level, refractive index of Si and the refractive index of the analyte material, respectively. Meanwhile, the refractive index of Si is a wavelength dependent that can be expressed according to Sellmeier dispersion formula as [35]:

$$n_{\mathrm{Si}}(\lambda) = \sqrt{\varepsilon_{\mathrm{Si}}} = \sqrt{1 + \frac{10.6684293\,\lambda^2}{\lambda^2 - 0.0909} + \frac{0.0034347484\,\lambda^2}{\lambda^2 - 1.2877} + \frac{1.54133408\,\lambda^2}{\lambda^2 - 1218816}} \tag{14}$$

Here, λ describes the wavelength of the incident electromagnetic waves [35]. Therefore, the indices of refraction (n_1 and n_2) of layers a and b can be investigated based on Eqs. (13) and (14).

Finally, the refractive index of the defect layer n_{d} can be expressed as a function of the volume fraction of *E. Coli* bacteria. In particular, the pure water of refractive index of 1.3323 is considered as the slandered reference towards the detection of *E. Coli* bacteria [18,32]. In this regard, the defect layer is filled with pure water, then the *E. Coli* bacteria of different volume fractions or concentrations is embedded inside this pure water. Therefore, the refractive index of the defect layer increases with the increase of *E. Coli* concentrations through the defect layer. Therefore, the refractive index of the defect layer can be expressed as a function of the volume fraction of *E. Coli* bacteria according to the following fitted relation:

$$n_{\mathrm{d}} = n_{\mathrm{w}} + k\, V_f \tag{15}$$

such that $n_{\mathrm{w}} = 1.3323$ defines the refractive index of pure water, $k = 0.0577$ is a constant value and V_f describes the concentration of the volume fraction of *E. Coli* inside the pure water.

3. Result and discussion

The suggested 1D APC was designed using the successive layers of different porosity and with a period $N = 10$ before and after the defect layer. The structure was analysed by considering that the defect layer is filled with the analyte material. In this regard, layers a and b are designed from porous silicon of different porosity. Thus, layers a and b are specified with indices of refraction n_1 and n_2 as well as thicknesses d_1 and d_2,

respectively. In this regard, n_1 and n_2 can be simulated based on Eqs. (13) and (14) besides the refractive index of the analyte material. Notably, the analyte material (*E. Coli*) of different concentrations can flow through the voids of porous Si layers and the defect layer as well. In contrast, the defect layer is designed from water of thickness d_d and refractive index $n_d = 1.33$ that can be then filled with the *E. Coli* samples. Therefore, the proposed design is configured as, $\mathrm{Si}(\mathrm{pSi_a}/\mathrm{pSi_b})^N/(\text{water sample})/(\mathrm{pSi_a}/\mathrm{pSi_b})^N\mathrm{Si}$. Actually, the choice of two Si layers of different porosity in the design of the suggested sensor is proposed because pores materials provide a massive number of pores, which in turn makes the flow of the analyte through the pores and the defect layer easy and convenient toward an accurate, simple, and efficient detection process. In particular, this strategy could lead to a higher level of interaction between the incident electromagnetic waves and the considered analyte, which in turns could give rise to an improved sensing performance. In addition, providing two Si layers of different porosity in the design of each unit cell of the suggested structure could introduce a good matching level during the experimental verification besides the diversity of pores and their surface area as well [34].

Meanwhile, the voids inside the pores besides the defect layer can be filled with *E. Coli* samples for monitoring them. In particular, the inclusion of the defect layer plays a promising role in the sensing and monitoring of the *E. Coli* samples. Accordingly, the breaking of the structure's periodicity gives rise to the generation of a resonant peak through the formed bandgap [36]. The emergence of this resonant peak is due to the localization of some photons of a specified wavelength inside the introduced PBG [8,10]. This resonant peak can be tuned using the changes in the properties of the defect layer, especially its thickness and refractive index [6,9]. Meanwhile, the position of the defect peak can be investigated based on the thickness and refractive index of the defect layer. In particular, the thickness of the defect layer should be comparable with the wavelength of the incident electromagnetic waves to receive this resonant mode [8,10]. Then, light wave incident normally on the structure, and the azimuthal number m was assumed to be zero to avoid computational complexity. The modified TMM was employed to study the reflectance spectrum of the proposed APC. First, the reflectance spectrum of the structure was studied by separately considering the defect layer filled with water, as shown in Fig. 2. Initially, the thicknesses of layers a and b are set as $d_1 = 50$ nm and $d_2 = 65$ nm, respectively. In addition, the porosity of these layers is considered as 0.7 and 0.4. Then, the thickness of the defect layer is chosen as $d_d = 65$ nm. In particular, in the upcoming figures, we have introduced a detailed optimization process to investigate the best performance of the designed sensor. Here, a band gap was obtained from 502 to 625 nm in the reflectance based on these values. The emergence of this PBG at these spectral wavelengths is due to the contrast in the refractive index between the two porous Si layers through each unit cell of the designed 1D APCs. Notably, the choice of the two porous Si layers with different porosity, *i.e.*, 0.4 and 0.7 will give rise to two different indices of refractions for layers a and b. Remarkably, a sharp dip (*i.e.*, a defect peak) within the band gap was perceived at 525.6 nm.

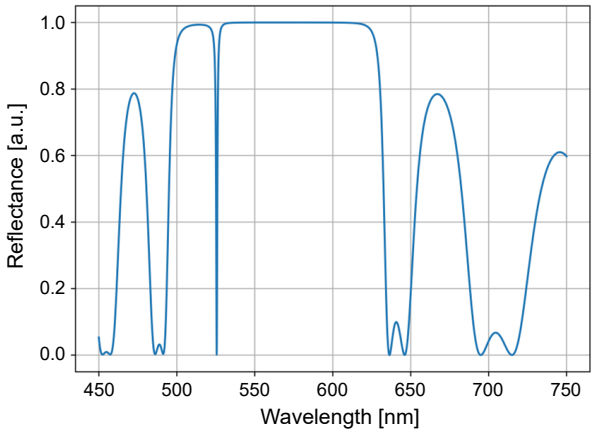

Fig. 2. Reflectance spectrum of the 1D APCs containing a defect layer filled with pure water.

Here, the emergence of the defect peak in this specified spectral wavelength is due to the filling of the defect layer with pure water. As the *E. Coli* bacteria of different concentration involved through pure water, the spectral position of this resonant peak is shifted towards the longer wavelengths [10]. Therefore, the mainstay of this study was to investigate the defect mode's characteristics concerning various changes in *E. Coli* volume fractions across the defect layer.

For this purpose, we have considered in what follows an optimization procedure of the different parameters towards the best performance of our *E. Coli* sensor. In this regard, Fig. 3 demonstrates the impact of the defect layer thickness on the properties of the defect peak and the performance of the designed *E. Coli* sensor as well. Figure 3(a) introduces the shift in the defect peak position due to the increase in the defect layer thickness. As the value of the defect layer thickness increases, the defect peak is red shifted upwards the longer wavelengths besides a little shift in the upper and lower edges of the PBG. This behaviour is due to the change of the optical path length with the increase in the thickness of the defect layer [36,37]. Thus, for an increase in the thickness of the defect layer, the shift in the position of the defect peak is expected. Then, Figs. 3(b)–(d) display the role of the defect layer thickness on the performance of the considered sensor. Figure 3(b) shows the response of the quality factor of our sensor *versus* the thickness of the defect layer at two different concentrations of the analyte material. It is worth noting that the quality factor of the designed sensor could be increased from 240 to 690 due to the increase in the value of d_d from 30 to 70 nm, respectively for pure water case. As the volume fraction of *E. Coli* through water of 0.5, the quality factor is almost unaffected receiving a value of 640 at a thickness of the defect layer of 70 nm. Here, the increase in the value of the quality factor with the increase in the thickness of the defect layer could be due to the decrease in the full width at half maximum and the shift in the resonance peak. In contrast, Figs. 3(c) and (d) investigate a significant increase in both sensitivity and figure of merit due to the

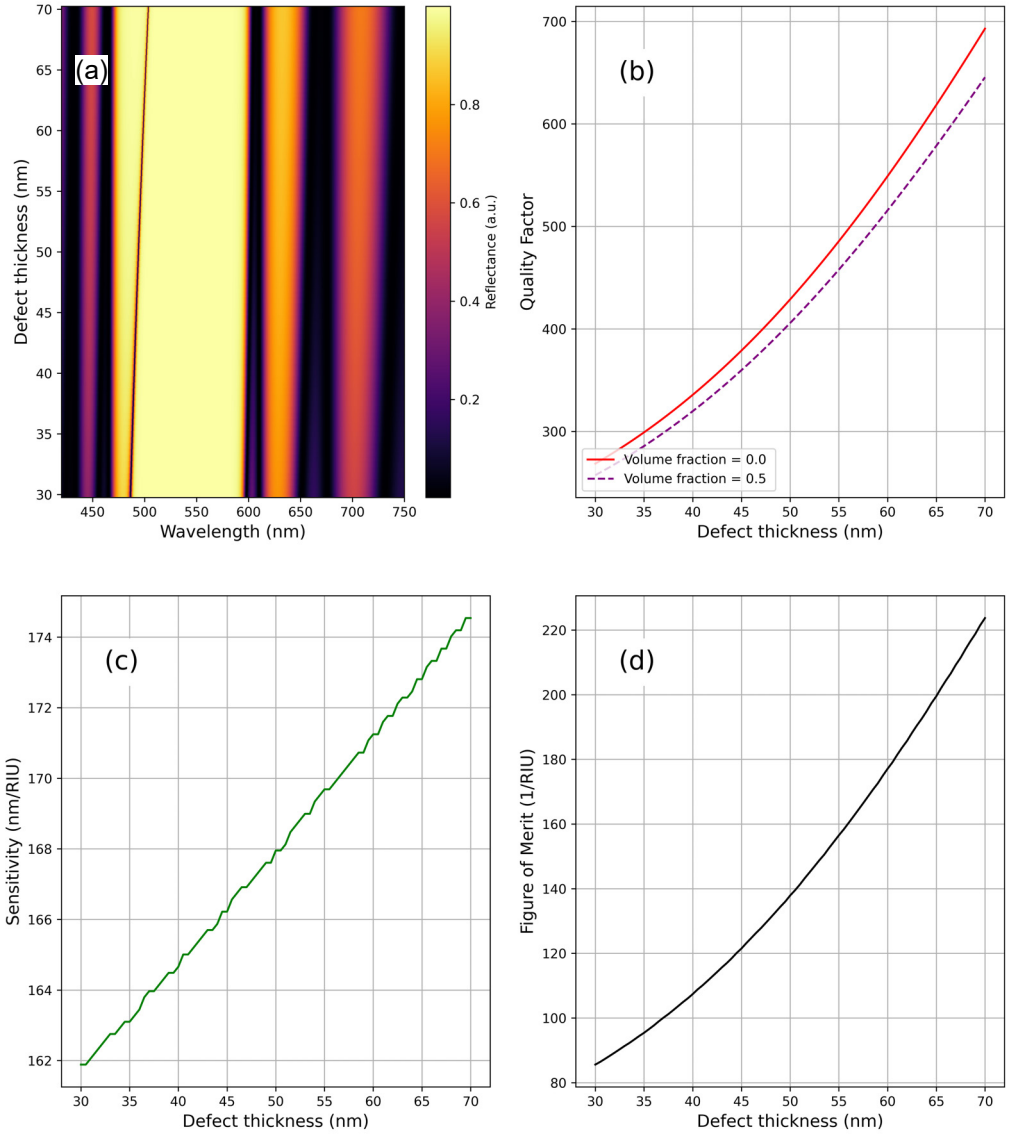

Fig. 3. (a) A colour map for the defect mode of the 1D APCs at various values of the defect layer's thickness, (b) the response of quality factor *vs*. the defect layer thickness, (c) the sensitivity's values of *E. Coli* sensor *vs*. the defect layer thickness, and (d) the figure of merit *vs*. the defect layer thickness.

increase in the value of d_d, respectively. As shown in Fig. 3(c), the sensitivity of the designed *E. Coli* sensor provides a linear increase with the defect layer thickness increasing. In this regard, the sensitivity increases from 161.9 to 174.6 nm/RIU as the thickness of the defect layer increases from 30 to 70 nm. However, the increase in d_d over 70 nm is not accepted because the full width at half maximum of the resonant peak becomes smaller than 0.8 nm. Therefore, measuring of other performance pa-

rameters such as quality factor and figure of merit is very difficult on both theoretical and experimental procedures. Therefore, a defect layer thickness of 70 nm represents the optimum value in our study.

Then, at an optimum thickness of 70 nm for the defect layer, Fig. 4 introduces the effect of the thickness of layer a on the performance of the designed sensor. Figure 4(a) shows a significant shift of both resonant peak and PBG towards the longer wave-

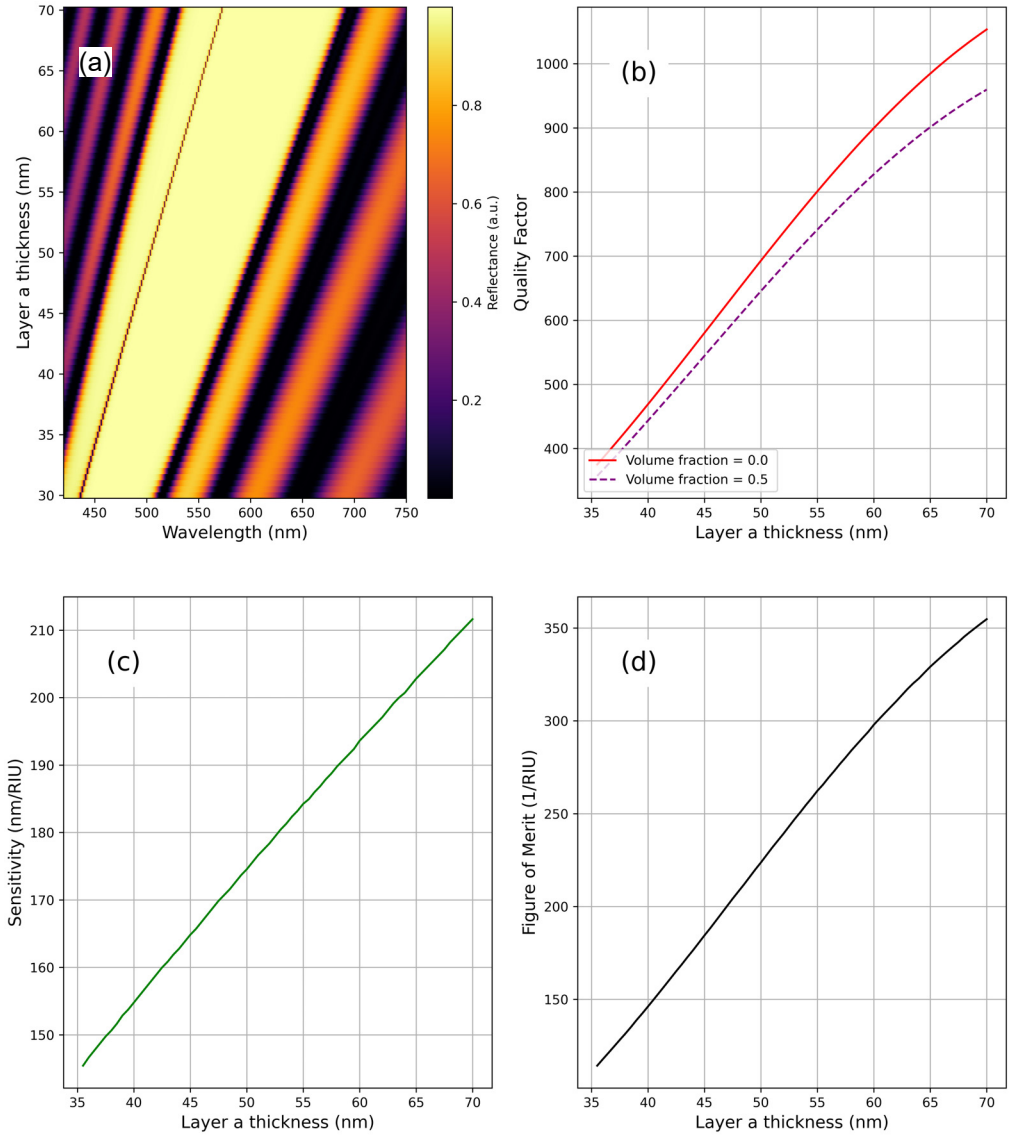

Fig. 4. (a) Reflectance of the APCs at different values of layer a thickness, (b) variation of quality factor's values *vs*. layer a thickness, (c) the sensitivity of the sensor *vs*. layer a thickness, and (d) the impact of layer a thickness on the figure of merit.

lengths with the increase in d_1 value from 35 to 70 nm due to the significant change in the path length of the interacting electromagnetic waves. This response can significantly improve the performance of the designed sensor in the vicinity of its sensitivity, quality factor and figure of merit as well. As shown in Fig. 4(b), the quality factor could receive a value of 1050 as the thickness of layer a = 70 nm. In addition, at d_1 = 70 nm, the sensitivity of the proposed sensor and figure of merit can be increased to 211 and 354 nm/RIU as shown in Figs. 4(c) and (d), respectively. For further increase of d_1 over 70 nm, the edges of the PBG loss their stability besides the emergence of some ripples which in turns could interfere with the resonant peak leading to a significant fluctuation through the detection procedure. Thus, 70 nm represents the optimum thickness of layer a.

In contrast, Fig. 5 shows the impact of changing the thickness of layer b on the sensor performance at constant values of d_1 = 70 nm and d_d = 70 nm. Similar to the previous results, the increase in the thickness of layer b provides a pronounced effect on both PBG properties and resonant peak as well. Here, the PBG is shifted with the increase of d_2 value towards the longer wavelengths with the emergence of its upper edge outside the considered spectrum region as shown in Fig. 5(a). In addition, the resonant peak is shifted from 472 to 610 nm with some decrease in its intensity due to the increase in the thickness of layer b from 40 to 75 nm, respectively. In contrast, the quality factor and figure of merit received considerable decrements in their values with the increase of d_2 value as shown in Figs. 5(b) and (d), respectively. This response could be due to the increase in the FWHM of the resonant peak with the thickness of layer b. However, the values of sensitivity provided a considerable increase receiving 221 nm/RIU at d_2 = 75 nm. Therefore, we have considered 75 nm for the thickness of layer b as an optimum value.

Therefore, thicknesses of d_1 = 70 nm, d_2 = 75 nm, d_d = 70 nm and porosity of layer a of 0.7 represent the optimum values of our designed sensor. In this regard, at the optimum values of the different parameters, we have considered in Fig. 6(a) the reflectance spectrum of the designed structure at different values of the volume fraction of *E. Coli* inside the pure water. The defect peak appeared within the band gap, and the wavelength of this defect peak continued to increase with an increase in the volume fraction of *E. Coli*. Such effect could be due to the change of the optical path length with the volume fraction (concentration) of *E. Coli* bacteria [36]. In other words, to keep the state of the phase shift condition, the increase in the refractive index of the defect layer due to the increase in the concentration of *E. Coli* samples in pure water leads to a profound increase in the position of the defect peak [37]. Thus, for an increase in the refractive index of the defect layer, the shift in the position of the defect peak is expected. Then, Fig. 6(b) displays the sensitivity of the designed *E. Coli* sensor *versus* the increase in its volume fraction. It is worth noting that the value of the sensitivity is almost constant with the change in the concentration of *E. Coli* bacteria in pure water. Notably, its value changes from 231.4 to 230.7 nm/RIU through the overall variation of *E. Coli* volume fraction. Therefore, we believe that our sensor could be of interest

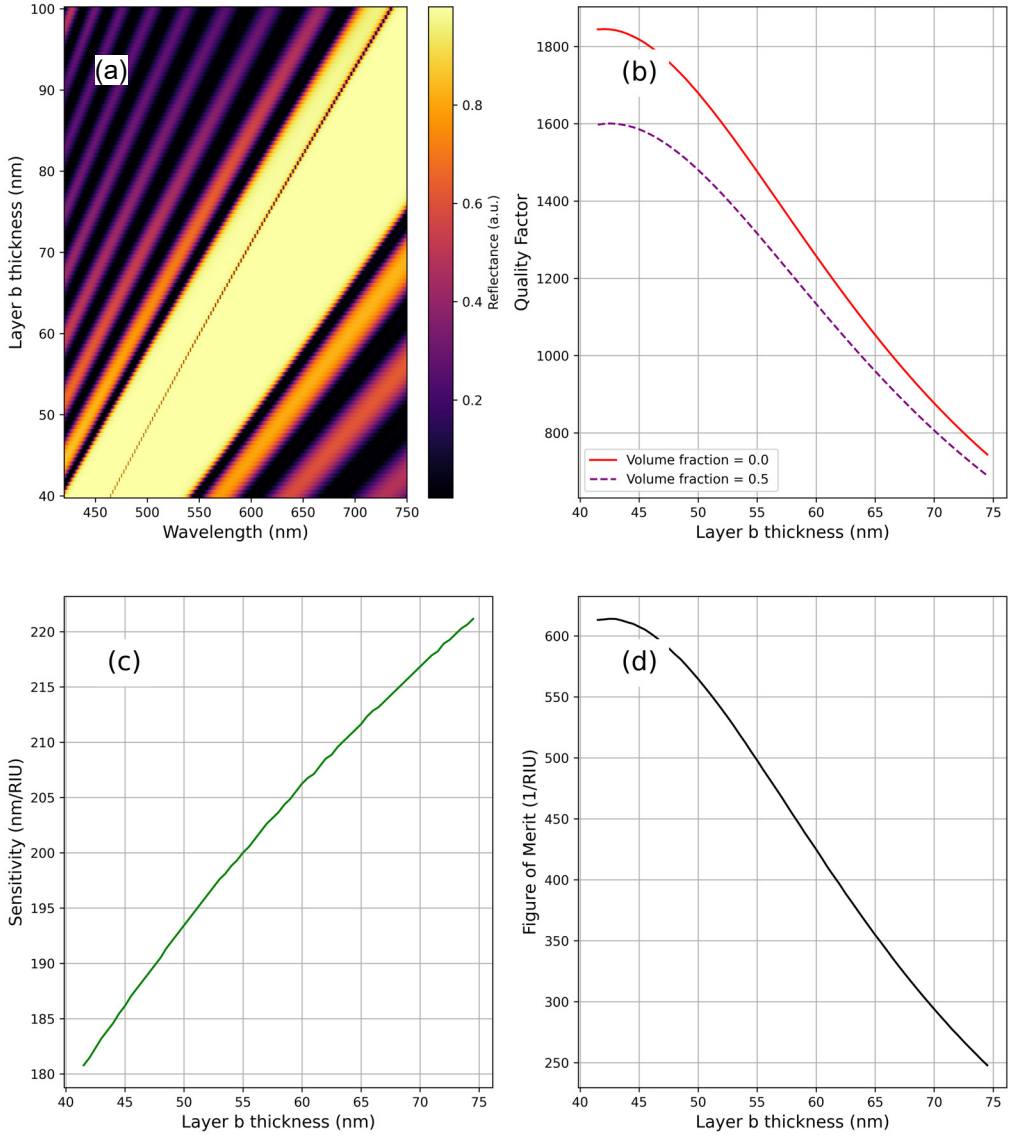

Fig. 5. (a) Reflectance of the APCs at different values of layer b thickness, (b) variation of quality factor's values *vs*. layer b thickness, (c) the sensitivity of the sensor *vs*. layer b thickness, and (d) the impact of layer b thickness on the figure of merit.

on the level of sensitivity's stability whatever the concentration of *E. Coli* bacteria in pure water.

Finally, we have introduced in the Table a brief comparison between the performance of our designed structure and some of the recently designed sensors based on PC structures in the vicinity of the achieved sensitivity. It is worth noting that our de-

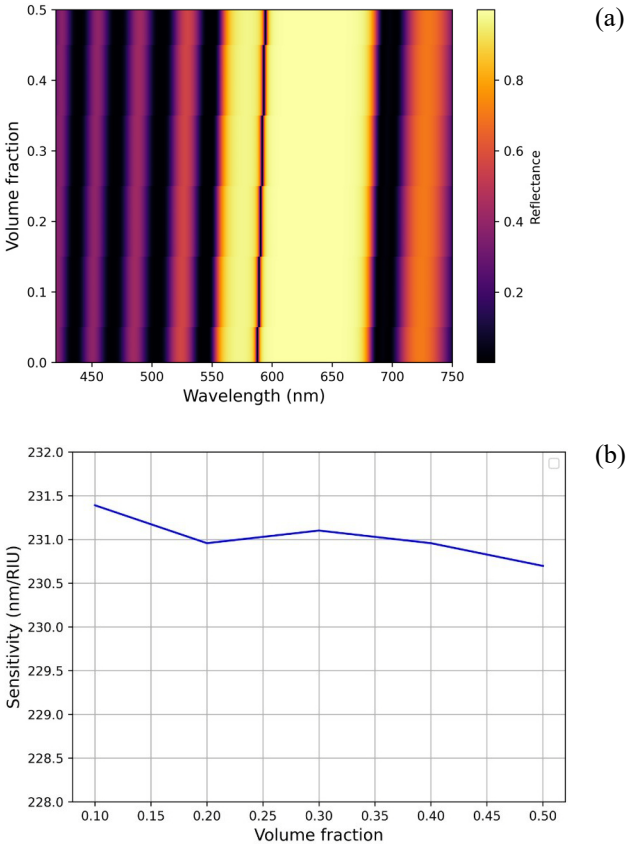

Fig. 6. (a) A colour map for the reflectivity of the 1D APC sensor at different volume fractions of *E. Coli* bacteria in pure water. (b) The sensitivity of the 1D APC sensor at different volume fractions of *E. Coli* bacteria in pure water.

signed 1D APC structure provides a good performance compared to some of its counterparts as listed in the Table because our proposed APC sensor outperforms in sensitivity over the others. In addition, the proposed design could be of interest for

T a b l e. A brief comparison between some of the earlier research using 1D defective planar PCs with the suggested 1D defective APCs.

Sensor design	The detected analyte	Sensitivity [nm/RIU]	Ref.
1D porous PCs	*E. Coli* bacteria in pure water	174	[18]
1D dielectric PCs	Biodiesel	136.8	[38]
1D nanocomposite coated PCs	Cancerous cells	43	[39]
1D binary PCs	Hemoglobin in blood plasma	72	[40]
1D binary PCs	Fat concentration in milk	106.7	[41]
Our 1D APC sensor	*E. Coli* in pure water	231.4	This work

fabrication procedure. Notably, for the 1D APC structures, the layers are arranged in a circular fashion, which makes the overall structure compact as compared to the regular 1D PCs besides its stability over the regular PC structures as well. Moreover, 1D APCs can be introduced as a non-intrusive and label-free method for optical sensing applications. Therefore, we believe that our introduced sensor presents a good choice, especially in the proposed 1D APC sensor which is compact in size and can be easily fitted in a small area as well.

4. Conclusion

In conclusion, this work thoroughly examines the design and functionality of a 1D APCs for pathogen identification. The APC structure consists of alternating silicon layers with varying porosities arranged in a periodic pattern. The incorporation of porous materials in APC design could enhance their applicability, particularly for sensing purposes. A defect layer has been introduced to facilitate the detection and monitoring of *E. Coli* bacteria. To achieve high performance, several optimization steps are performed for key geometrical parameters. Various performance metrics, such as resonant peak position, quality factor, and sensitivity, are calculated. The sensor exhibits a high -quality factor of 667.5 and a sensitivity of 231.4 nm/RIU, underscoring its ability to reliably differentiate between various infections. These results, along with the potential for integrating the APC with other diagnostic methods, suggest that this technology could significantly enhance the prevention and control of infectious diseases. Moreover, we believe that the designed sensor could be of a significant interest as a good indicator for some chemical and biological microfluidic components.

Acknowledgment
The authors extend their appreciation to King Saud University for funding this work through Researchers Supporting Project number (RSP2025R133), King Saud University, Riyadh, Saudi Arabia.

References

[1] Shaban M., Ahmed A.M., Abdel-Rahman E., Hamdy H., *Tunability and sensing properties of plasmonic/1D photonic crystal*, Scientific Reports **7**, 2017: 41983. https://doi.org/10.1038/srep41983

[2] Xia Y., Kamata K., Lu Y., *Photonic crystals*, [In] Di Ventra M., Evoy S., Heflin J.R. [Eds.] *Introduction to Nanoscale Science and Technology*, Nanostructure Science and Technology, Springer, Boston, MA, 2004. https://doi.org/10.1007/1-4020-7757-2_21

[3] Cersonsky R.K., Antonaglia J., Dice B.D., Glotzer S.C., *The diversity of three-dimensional photonic crystals*, Nature Communications **12**, 2021: 2543. https://doi.org/10.1038/s41467-021-22809-6

[4] Devashish D., Ojambati O.S., Hasan S.B., van der Vegt J.J.W., Vos W.L., *Three-dimensional photonic band gap cavity with finite support: Enhanced energy density and optical absorption*, Physical Review B **99**(7), 2019: 075112. https://doi.org/10.1103/PhysRevB.99.075112

[5] Aghajamali A., Barati M., *Effects of normal and oblique incidence on zero-$\overline{n}$ gap in periodic lossy multilayer containing double-negative materials*, Physica B: Condensed Matter **407**(8), 2012: 1287 -1291. https://doi.org/10.1016/j.physb.2012.01.125

[6] ZHU C.Y., ZHANG Z., QIN J.K., WANG Z., WANG C., MIAO P., LIU Y., HUANG P.Y., ZHANG Y., XU K., ZHEN L., CHAI Y., XU C.Y., *Two-dimensional semiconducting SnP_2Se_6 with giant second-harmonic -generation for monolithic on-chip electronic-photonic integration*, Nature Communications **14**, 2023: 2521. https://doi.org/10.1038/s41467-023-38131-2

[7] KUMAR A., KUMAR N., THAPA K.B., *Tunable broadband reflector and narrowband filter of a dielectric and magnetized cold plasma photonic crystal*, The European Physical Journal Plus **133**, 2018: 250. https://doi.org/10.1140/epjp/i2018-12073-3

[8] LIN Y.C., CHOU S.H., HSUEH W.J., *Robust high-Q filter with complete transmission by conjugated topological photonic crystals*, Scientific Reports **10**, 2020: 7040. https://doi.org/10.1038/s41598 -020-64076-3

[9] YOUNG A.B., THIJSSEN A.C.T., BEGGS D.M., ANDROVITSANEAS P., KUIPERS L., RARITY J.G., HUGHES S., OULTON R., *Polarization engineering in photonic crystal waveguides for spin-photon entanglers*, Physical Review Letters **115**(15), 2015: 153901. https://doi.org/10.1103/PhysRevLett.115.153901

[10] KHANI S., HAYATI M., *Optical biosensors using plasmonic and photonic crystal band-gap structures for the detection of basal cell cancer*, Scientific Reports **12**, 2022: 5246. https://doi.org/10.1038/ s41598-022-09213-w

[11] CHANG T.-W., HSU H.-T., WU C.-J., *Investigation of photonic band gap in a circular photonic crystal*, Journal of Electromagnetic Waves and Applications **25**(16), 2011: 2222-2235. https://doi.org/ 10.1163/156939311798147123

[12] BOUFENAR R., BOUAMAR M., HOCINI A., *Numerical analysis of a temperature sensor based on the photonic band gap effect in a photonic crystal fiber*, Chinese Journal of Physics **56**(3), 2018: 1126 -1132. https://doi.org/10.1016/j.cjph.2018.03.036

[13] EL-AMASSI D.M., TAYA S.A., VIGNESWARAN D., *Temperature sensor utilizing a ternary photonic crystal with a polymer layer sandwiched between Si and SiO2 layers*, Journal of Theoretical and Applied Physics **12**(4), 2018: 293-298. https://doi.org/10.1007/s40094-018-0308-x

[14] LIU Q., PENG H., LU X., LE X.C., *Enzyme-assisted extraction and liquid chromatography mass spectrometry for the determination of arsenic species in chicken meat*, Analytica Chimica Acta **888**, 2015: 1-9. https://doi.org/10.1016/j.aca.2015.05.001

[15] CHANG Y.-H., JHU Y.-Y., WU C.-J., *Temperature dependence of defect mode in a defective photonic crystal*, Optics Communications **285**(6), 2012: 1501-1504. https://doi.org/10.1016/j.optcom.2011. 10.053

[16] HU C.-A., WU C.-J., YANG T.-J., YANG S.-L., *Analysis of optical properties in cylindrical dielectric photonic crystal*, Optics Communications **291**, 2013: 424-434. https://doi.org/10.1016/j.optcom. 2012.11.042

[17] SRIVASTAVA S.K., AGHAJAMALI A., *Investigation of reflectance properties in 1D ternary annular photonic crystal containing semiconductor and high-T_c superconductor*, Journal of Superconductivity and Novel Magnetism **29**, 2016: 1423-1431. https://doi.org/10.1007/s10948-016-3413-6

[18] HAO J.J., XIE X., GU K.D., DU W.C., LIU Y.J., YANG H.W., *Research on photonic crystal-based biosensor for detection of* Escherichia coli *colony*, Plasmonics **14**, 2019: 1919-1928. https://doi.org/ 10.1007/s11468-019-00987-w

[19] MAJI P.S., SHUKLA M.K., DAS R., *Blood component detection based on miniaturized self-referenced hybrid Tamm-plasmon-polariton sensor*, Sensors and Actuators B: Chemical **255**, 2018: 729-734. https://doi.org/10.1016/j.snb.2017.08.031

[20] ZHANG X., ZHU X.-S., SHI Y.-W., *An optical fiber refractive index sensor based on the hybrid mode of Tamm and surface plasmon polaritons*, Sensors **18**(7), 2018: 2129. https://doi.org/10.3390/ s18072129

[21] ZHANG X.-L., FENG J., HAN X.-C., LIU Y.-F., CHEN Q.-D., SONG J.-F., SUN H.-B., *Hybrid Tamm plasmon-polariton/microcavity modes for white top-emitting organic light-emitting devices*, Optica **2**(6), 2015: 579-584. https://doi.org/10.1364/OPTICA.2.000579

[22] Zhang X.-L., Song J.-F., Feng J., Sun H.-B., *Spectral engineering by flexible tunings of optical Tamm states and Fabry–Perot cavity resonance*, Optics Letters **38**(21), 2013: 4382-4385. https://doi.org/10.1364/OL.38.004382

[23] Klimov V.V., Pavlov A.A., Treshin I.V., Zabkov I.V., *Fano resonances in a photonic crystal covered with a perforated gold film and its application to bio-sensing*, Journal of Physics D: Applied Physics **50**(28), 2017: 285101. https://doi.org/10.1088/1361-6463/aa75e6

[24] Sayed H., Swillam M.A., Aly A.H., *Annular one-dimensional photonic crystals for salinity sensing*, Scientific Reports **13**, 2023: 20593. https://doi.org/10.1038/s41598-023-47205-6

[25] Abadla M.M., Elsayed H.A., Mehaney A., *Thermo-optical properties of binary one dimensional annular photonic crystal including temperature dependent constituents*, Physica E: Low-dimensional Systems and Nanostructures **119**, 2020: 114020. https://doi.org/10.1016/j.physe.2020.114020

[26] Abadla M.M., Elsayed H.A., Mehaney A., *Sensitivity enhancement of annular one dimensional photonic crystals temperature sensors with nematic liquid crystals*, Physica Scripta **95**(8), 2020: 085508. https://doi.org/10.1088/1402-4896/aba2b0

[27] Gandhi S., Awasthi S.K., *Detection of wide variety of pathogens by using one-dimensional biosensor based on annular photonic crystal*, Materials Today: Proceedings, 2023. https://doi.org/10.1016/j.matpr.2023.05.203

[28] Ioannidis N., Cooper C.E., Poole R.K., *Spectroscopic studies on an oxygen-binding haemoglobin-like flavohaemoprotein from* Escherichia coli, Biochemical Journal **288**(2), 1992: 649-655. https://doi.org/10.1042/bj2880649

[29] Hariri S., *Detection of* Escherichia coli *in food samples using culture and polymerase chain reaction methods*, Cureus **14**(12), 2022: e32808. https://doi.org/10.7759/cureus.32808

[30] Gally D.L., Stevens M.P., *Microbe profile:* Escherichia coli *O157:H7 – notorious relative of the microbiologist's workhorse*, Microbiology **163**(1), 2017: 1-3. https://doi.org/10.1099/mic.0.000387

[31] Lim J.Y., Yoon J.W., Hovde C.J., *A brief overview of* Escherichia coli *O157:H7 and its plasmid O157*, Journal of Microbiology and Biotechnology **20**(1), 2010: 5-14.

[32] Xin H.B., Li Y.Y., Liu X.S., Li B.J., Escherichia coli-*based biophotonic waveguides*, Nano Letters **13**(7), 2013: 3408-3413. https://doi.org/10.1021/nl401870d

[33] Lin X., Zhao M., Peng T., Zhang P., Shen R., Jia Y., *Detection and discrimination of pathogenic bacteria with nanomaterials-based optical biosensors: A review*, Food Chemistry **426**, 2023: 136578. https://doi.org/10.1016/j.foodchem.2023.136578

[34] Chourasiaa R.K., Yadavb C.S., Upadhyay A., Chourasiac N.K., Singh V., *Analysis of Bragg fiber waveguides having a defect layer for biosensing applications*, Optik **200**, 2020: 163400. https://doi.org/10.1016/j.ijleo.2019.163400

[35] Tatian B., *Fitting refractive-index data with the Sellmeier dispersion formula*, Applied Optics **23**(24), 1984: 4477-4485. https://doi.org/10.1364/AO.23.004477

[36] Rashwan H.H., Mostafa S.I., El-Khawas E.H., El-Naggar S.A., *Tunable filter based on one-dimensional photonic crystal including nanocomposite material*, The European Physical Journal D **76**, 2022: 50. https://doi.org/10.1140/epjd/s10053-022-00373-y

[37] Mehaney A., Alrowaili Z.A., Elsayed H.A., Taha T.A., Ahmed A.M., *Theoretical investigations of Tamm plasmon resonance for monitoring of isoprene traces in the exhaled breath: Towards chronic liver fibrosis disease biomarkers*, Physics Letters A **413**, 2021: 127610. https://doi.org/10.1016/j.physleta.2021.127610

[38] Elsayed H.A., Mehaney A., *Theoretical verification of photonic crystals sensor for biodiesel detection and sensing*, Physica Scripta **95**(8), 2020: 085507. https://doi.org/10.1088/1402-4896/aba2b1

[39] Ramanujam N.R., Amiri I.S., Taya S.A., Olyaee S., Udaiyakumar R., Pasumpon Pandian A., Wilson K.S.J., Mahalakshmi P., Yupapin P.P., *Enhanced sensitivity of cancer cell using one dimensional nano composite material coated photonic crystal*, Microsystem Technologies **25**, 2019: 189-196. https://doi.org/10.1007/s00542-018-3947-6

[40] BIJALWAN A., SINGH B.K., RASTOGI V., *Analysis of one-dimensional photonic crystal based sensor for detection of blood plasma and cancer cells*, Optik **226**, 2021: 165994. https://doi.org/10.1016/j.ijleo.2020.165994
[41] ABOHASSAN K.M., ASHOUR H.S., ABADLA M.M., *A 1D binary photonic crystal sensor for detecting fat concentrations in commercial milk*, RSC Advances **11**(20), 2021: 12058-12065. https://doi.org/10.1039/D1RA00955A

Received February 24, 2025